

ORIGINAL RESEARCH

Open Access



Preparation of carbon-based material with high water absorption capacity and its effect on the water retention characteristics of sandy soil

Youming Yang^{1,2}, Mingyang Zhong^{1,2}, Xiuqi Bian^{1,2}, Yongjun You^{1,2} and Fayong Li^{1,2*} 

Abstract

Biochar has the potential to provide a multitude of benefits when used in soil remediation and increasing soil organic matter enrichment. Nevertheless, the intricate, hydrophobic pores and groups weaken its water-holding capacity in dry, sandy soils in arid lands. In order to combat this issue, starch-carbon-based material (SB), sodium alginate-carbon-based material (SAB), and chitosan-carbon-based material (CB) have been successfully synthesized through the graft-polymerization of biochar (BC). A series of soil column simulations were used to scrutinize the microstructure of the carbon-based material and explore its water absorption properties and its effects on sandy soil water infiltration, water retention, and aggregation. The results indicated that SB, SAB, and CB achieved water maximum absorption rates of 155, 188, and 172 g g⁻¹, respectively. Considering their impact on sandy soils, SB, SAB, and CB lengthened infiltration times by 1920, 3330, and 3880 min, respectively, whilst enhancing the water retention capabilities of the soil by 18%, 25%, and 23% in comparison to solely adding BC. The utilization of these innovative materials notably encouraged the formation of sandy soil aggregates ranging from 2.0 to 0.25 mm, endowing the aggregates with enhanced structural stability. Findings from potting experiments suggested that all three carbon-based materials were conducive to the growth of soybean seeds. Thus, it is evident that the carbon-based materials have been fabricated with success, and they have great potential not only to significantly augment the water retention capacities and structural robustness of sandy soils in arid areas, but also to bolster the development of soil aggregates and crop growth. These materials possess significant application potential for enhancing the quality of sandy soils in arid and semi-arid regions.

Highlights

- Novel carbon-based materials were prepared using biochar and biodegradable organic matter.
- The novel materials exhibited excellent water absorption capacity.
- The novel materials greatly decreased the water infiltration capacity of sandy soil.
- The novel materials increased the water retention capacity and aggregate size of sandy soils.

Handling editor: Xiaoyuan Yan.

*Correspondence:

Fayong Li
lisen8279@163.com

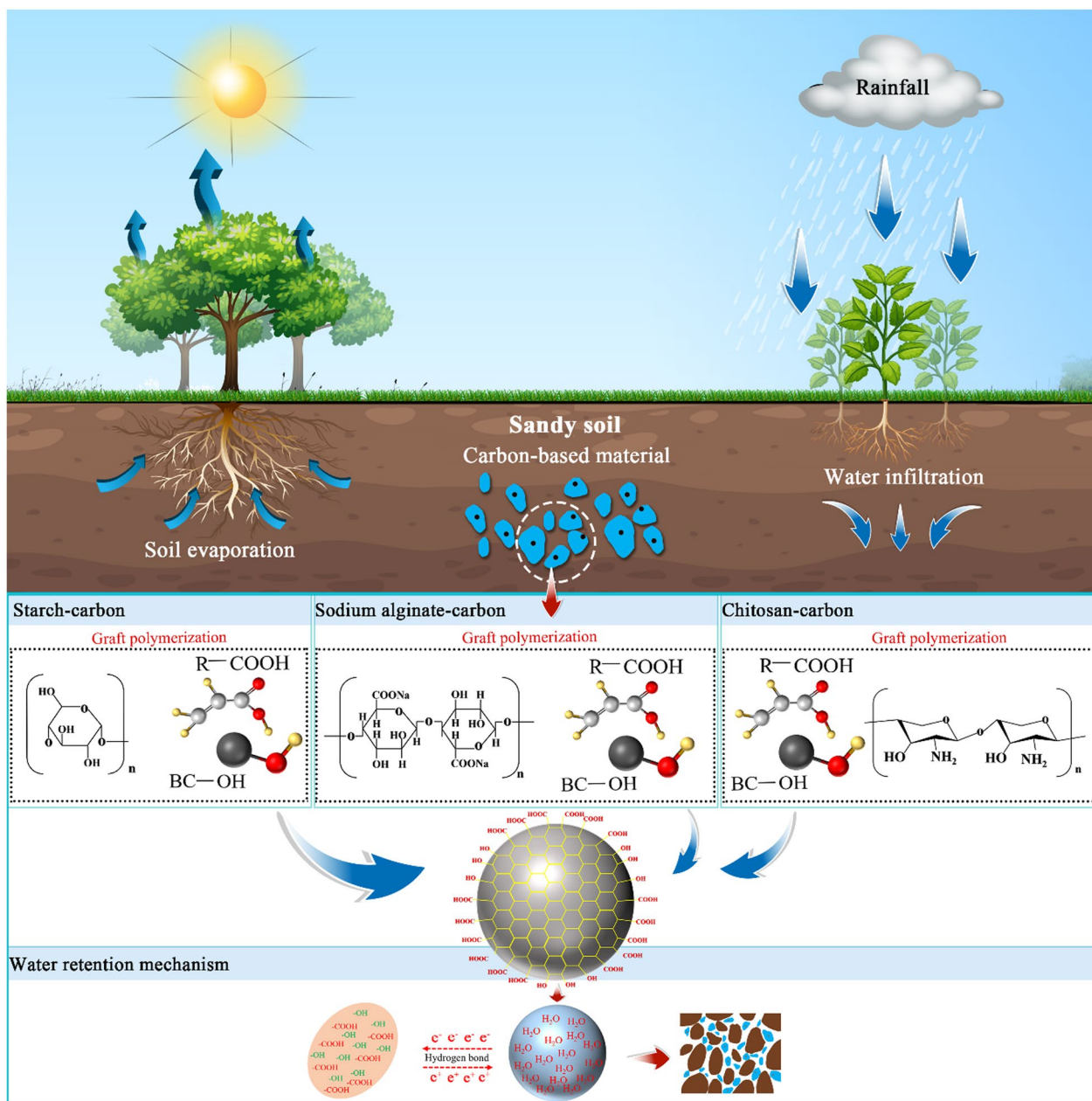
Full list of author information is available at the end of the article



© The Author(s) 2023. **Open Access** This article is licensed under a Creative Commons Attribution 4.0 International License, which permits use, sharing, adaptation, distribution and reproduction in any medium or format, as long as you give appropriate credit to the original author(s) and the source, provide a link to the Creative Commons licence, and indicate if changes were made. The images or other third party material in this article are included in the article's Creative Commons licence, unless indicated otherwise in a credit line to the material. If material is not included in the article's Creative Commons licence and your intended use is not permitted by statutory regulation or exceeds the permitted use, you will need to obtain permission directly from the copyright holder. To view a copy of this licence, visit <http://creativecommons.org/licenses/by/4.0/>.

Keywords Biochar, Water retention capacity, Water absorption rate, Infiltration, Soil moisture

Graphical Abstract



1 Introduction

Land desertification, an alarming environmental issue rampant in arid and semi-arid regions, significantly hampers agricultural productivity and human development. It rapidly transforms feasible land into sandy,

unproductive soils (Zhang et al. 2019). Globally, the area covered by sandy soils reached 4.99×10^7 km², accounting for 31% of the global total land area (Hengl et al. 2017). Up to 2014, China has had a sandy soil area of 1.72×10^6 km², or 17.93% of its total area (Pu et al. 2019). Xinjiang

province has the largest sandy soil expanse with a total of 7.47×10^5 km², accounting for two-fifths of the country's sandy soil (Lv et al. 2022). Owing to its geological and climatic conditions, the region experiences scarce rainfall and high evaporation rates. Combined with human's irrational utilization of natural resources, these factors have significantly deteriorated the soil quality, damaged its structure and severely weakened its capacity for water retention. Consequently, soil desiccation has become markedly more severe (Yu et al. 2022). Therefore, it is crucial to execute forceful measures to combat soil erosion and abate desertification by improving the physical and hydraulic properties of sandy soils and boosting their water retention ability. In recent years, researchers have proposed a handful of approaches for enhancing water retention in sandy soils, like application of super-absorbent materials (Albalasmeh et al. 2021), organic fertilizers (Iqbal et al. 2018), and inorganic amendments (Zhang et al. 2020) to the sandy soil, which could notably reduce water loss and enhance nutrient levels (Huang and Hartemink 2020). Nevertheless, the majority of absorbent materials exhibit resistant to biodegradation and certain chemical agents used for water storage may harbor toxic implications for both plants and soils (Xi and Zhang 2021), thereby posing potential risks to human health and the environment. Besides, inorganic amendments are relatively costly and hence inapplicable for large-scale application. As a result, the production of cost-effective and eco-friendly soil conditioners is of paramount importance.

Over the past decade, biochar has garnered substantial attention as an auspicious soil additive, attributed to its intricate pore structure, expansive specific surface area, and the presence of polycyclic aromatic hydrocarbons combined with polar functional groups (Downie et al. 2012; Weber and Quicker 2018). Research has found that biochar can increase organic carbon content in sandy soils (Parihar et al. 2016), bolster soil aggregation potential, foster superior soil particle aggregation, and improve soil structure (Baiaamonte et al. 2019). Furthermore, biochar with higher application rates, smaller particle sizes, and high porosity is seen to diminish the bulk weight of sandy soils, improve their water retention ability, and influence water infiltration in sandy soils (Verheijen et al. 2019; Alghamdi et al. 2020; Liu et al. 2016, 2017). However, most existing research posits that biochar, rather than enhancing, actually diminishes the water retention capability of soil. It has been determined that biochar introduction results in a rise in the soil's saturated hydraulic conductivity and a reduction in its cumulative infiltration (Mao et al. 2019; Phillips et al. 2020; Chen et al. 2022). Biochar itself is highly hydrophobic, which increases with

decreasing particle size and specific surface area, subsequently causing a decrease in biochar's water-holding capacity (Edeh and Mašek 2022). In sandy soils, biochar appears to have negligible effects on the water-holding capacity, saturated hydraulic conductivity, and effective plant water content (Wiersma et al. 2020). Chintala et al. (2014) discovered that biochar derived from corn straw and willow jig exhibits superior hydrophobicity, devoid of any water retention capabilities. Additionally, biochar has been found to expedite nutrient leaching from coarse-textured soils, thereby reducing their capacity to retain nutrients (Jílková and Angst 2022). In short, the influence of biochar on soil hydraulic properties depends on its raw material, pyrolysis process, particle size and application rate, as well as internal pore structure, specific surface area and hydrophobic groups content, with its capacity to retain water being markedly limited. When utilized in sandy soils, biochar might potentially exacerbate the loss of soil nutrients and water.

Therefore, in order to improve the water retention capacity of biochar in sandy soil, this study selected starch, sodium alginate, and chitosan polysaccharide substances as reaction monomers along with acrylic monomers. These substances were grafted onto biochar to create water-retaining polymer, thereby increasing the water retention capacity of biochar. Starch, sodium alginate, and chitosan polysaccharides offer the benefits of sustainability, biodegradability, and non-toxicity (Sutradhar et al. 2015). Rich in hydrophilic functional groups, they are the main components of naturally occurring complexes with high water-absorbent capacities, characterized by an abundance of hydrophilic functional groups (Campos et al. 2015; Guilherme et al. 2015). We hypothesized that the three carbon-based materials prepared in this study have undergone successful cross-linking and polymerization, resulting in their excellent water absorption properties. These properties have the potential to decelerate water infiltration in sandy soils, enhance the water retention capacity of such soils, facilitate the formation of large aggregates, and promote greater stability in the soil structure. The primary objectives of this study are as follows: (1) to examine the water absorption properties of the three carbon-based materials, (2) to validate the successful grafting of these materials through SEM, elemental analysis (EA), FT-IR, and contact angle characterization techniques, and (3) to investigate the impacts of the three carbon-based materials on water infiltration, water retention properties, and soil aggregates in sandy soils. Our results showed water retention abilities of biochar was enhanced, which can provide theoretical and technological support for sandy soil reclamation and water and soil conservation in arid areas.

2 Materials and methodology

2.1 Soil collection and preparation and carbon-based material preparation

2.1.1 Soil collection and preparation

Test soil was collected from cotton field in the water-saving irrigation experimental base of Tarim University, Alaer, Xinjiang (40° 20′ 47″–41° 47′ 18″ N, 79° 22′ 33″–81° 53′ 45″ E), which was collected from a depth of 0–20 cm. The collected soil was air-dried at room temperature and then sieved using a 2-mm mesh to remove debris and larger particles. The resultant soil was stored in a dry, clean container until use. It was recognized that the soil particle composition consisted of 75.58% fine sandy, 24.03% silt, and 0.39% clay, with a sandy loamy texture. Further analysis showed that the electrical conductivity was 1.14 mS cm⁻¹ and the pH level was 7.40. The soil's organic matter content was 11.14 g kg⁻¹, while its bulk density stood at 1.40 g cm⁻³, with a saturated moisture level of 43%.

2.1.2 Biochar preparation

The cotton straw was naturally dried indoors before being processed in a crusher machine (800A, Multifunctional Crusher, Dongguan Huatai Electric Co., Ltd.) for pulverization. The pulverized material was pyrolyzed in an oxygen-free environment using a muffle furnace (KSW, Box Type Resistance Furnace, Beijing Yongming Medical Instruments Co., Ltd.) at a temperature of 600 °C, with a heating rate of 8 °C min⁻¹ for 4 h to obtain biochar. The biochar was further ground and passed through a 60-mesh sieve, then collected and stored in a sealed wide-mouth bottle. It was dried before utilization to inhibit the absorption of airborne moisture into the material.

2.1.3 Carbon-based material synthesis

This study attempted to dissolve 0.5 g of chitosan (industrial grade, procured from Shandong Okang Biotechnology Co., Ltd.), in 30 mL of 2.0% mass fraction acetic acid solution (analytical purity), purchased from Shanghai Maclean Biochemical Technology Co., Ltd. This mixture was placed on a magnetic stirrer at an 800 r min⁻¹ speed, and the temperature was elevated to 70 °C. Subsequently, 0.08 g of *N,N'*-methylene bis(acrylamide) (MBA, analytical purity), procured from Shanghai Maclean Biochemical Technology Co., Ltd., and 12 mL of analytical purity acrylic acid (AA), provided by Fuchen (Tianjin) Chemical Reagent Co., Ltd., were integrated. The reaction was allowed to proceed for 10 min. Grafting polymerization reaction continued with the addition of 0.3 g ammonium persulfate (analytical purity, supplied by Tianjin Shengao Chemical Reagent Co., Ltd.) and 0.75 g of biochar,

and the reaction sustained for 40 min. Finally, sodium hydroxide (analytical purity, acquired from Tianjin Yongda Chemical Reagent Co., Ltd.) solution was added to accomplish hydrolysis, and the complex was cooled to the room temperature. The resultant product was a gelatinous complex, which was soaked in 99.70% ethanol for 24 h to remove unreacted monomers. This was followed by repeated rinsing with distilled water and drying at 60 °C. The ultimate chitosan-carbon-based material (CB) was obtained by pulverizing the complex into a powdery substance below 60-mesh diameter. The carbon-based material was subsequently preserved in a hermetically sealed wide-mouth bottle, and it was dried before utilization to inhibit the absorption of airborne moisture into the material. Figure 1 shows the grafting polymerization process (Baki and Abedi-Koupai 2018; Diao et al. 2014; Liu et al. 2021; Noordin et al. 2020; Wang et al. 2021).

Analogously, starch-carbon-based material (SB) and sodium alginate-carbon-based material (SAB) were prepared using the above method. However, the differences were in the solvent used (distilled water) and the amounts of *N,N'*-methylene bis(acrylamide) (MBA), acrylic acid (AA), and biochar, with 0.08 g MBA, 10 mL AA, and 0.75 g biochar for SB, and 0.07 g MBA, 10 mL AA, and 0.5 g biochar, respectively, for SAB.

2.2 Material characteristics

2.2.1 Grafting parameters

The grafting rate (G%) and grafting efficiency (E%) as parameters for characterizing the copolymer properties were ascertained using Eqs. (1) and (2), respectively.

$$\text{Grafting ratio \%} = \frac{W_g - W_0}{W_0}, \quad (1)$$

$$\text{Grafting efficiency \%} = \frac{W_g - W_0}{W_1}, \quad (2)$$

where W_g is the weight of the grafted polymer, W_0 is the weight of sodium alginate, chitosan and starch, respectively, and W_1 is the mass of the monomer.

2.2.2 Material characterization

The functional groups on the surface of carbon-based materials were analyzed using Fourier Transform Infrared Spectroscopy (FT-IR, Thermo Scientific Nicolet iS20, USA) within the frequency range of 4000–500 cm⁻¹. The surface morphological structure was assessed using Scanning Electron Microscopy (SEM, ZEISS Gemini 300, Germany). An Organic Elemental Analyzer (EA, Elementar UNICUBE, Germany) was utilized to determine the percentage of Carbon (C), Nitrogen (N), Oxygen (O), and Hydrogen (H) in the samples. Contact angle was

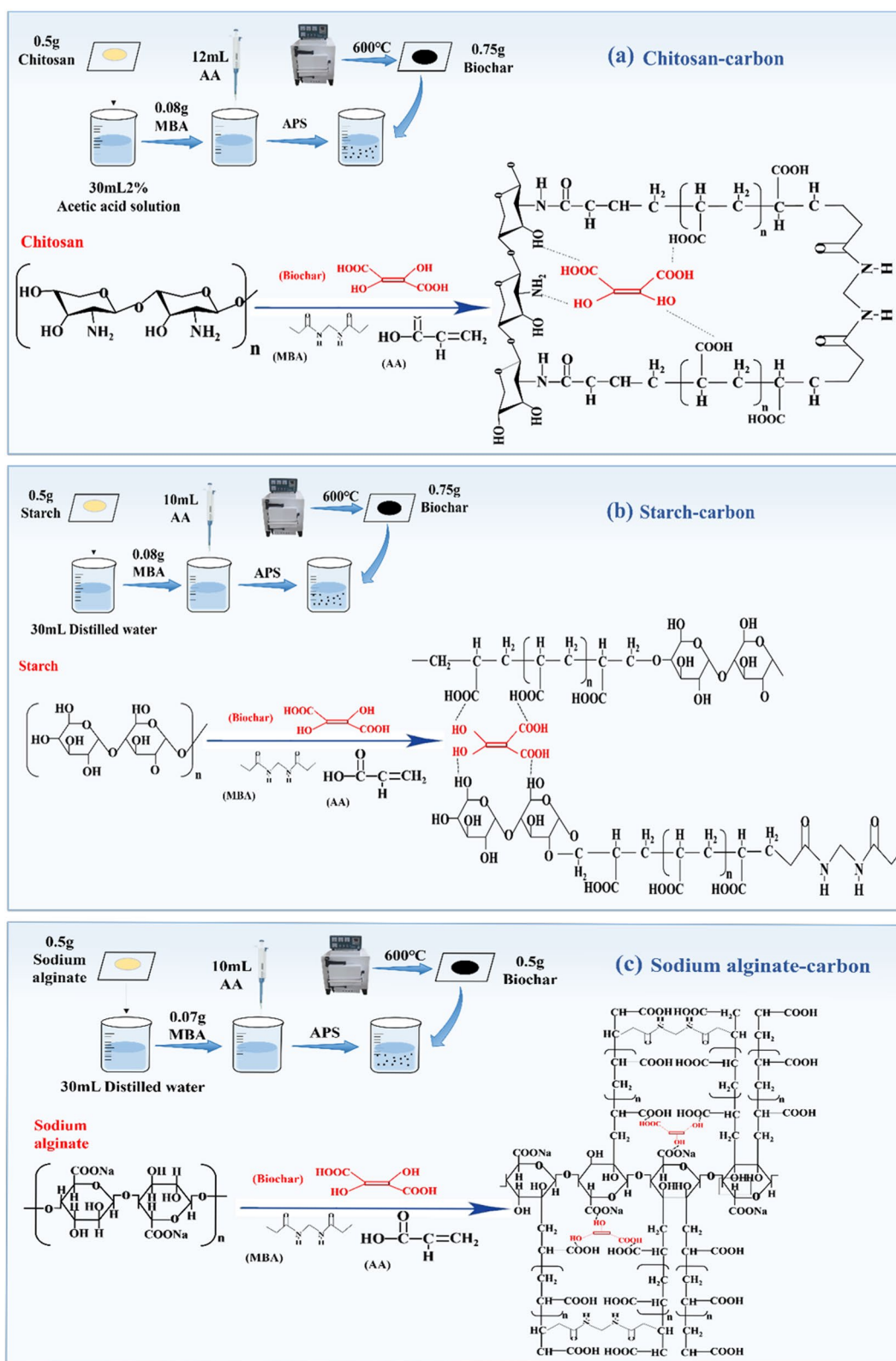


Fig. 1 Graft polymerization of biochar with chitosan, starch and sodium alginate, **a** Graft polymerization of biochar and chitosan, **b** Graft polymerization of biochar and starch, **c** Graft polymerization of biochar and sodium alginate

determined with a Surface tension tester (CA, JY-82C, China).

2.3 Experimental design

2.3.1 Measurement of water absorption capacity

A total of 0.1 g of BC, SB, SAB, and SB were completely immersed in 100 mL of distilled water, tap water and 0.9 wt% NaCl, respectively, for a period of 12 h at room temperature to ensure saturation. The saturated samples were subsequently filtered using a 100-mesh sieve to separate the saturated, swollen samples from the aqueous solution. They were then left to stand for 15 min to allow the excess water to be removed, after which both the sieve and the swollen samples were weighed simultaneously. The water absorption multiplicity was determined from the weight difference of the sample before and after its equilibrium water absorption and the experiment was repeated three times to be calculated as demonstrated by Eq. (3) (Xu et al. 2015).

$$W_A = \frac{W_S - W_d}{W_d}, \quad (3)$$

where W_A is the water absorption multiplicity per gram of dried carbon-based material, g g^{-1} . W_d and W_S are the weights of the materials after drying and water absorption saturation, g, respectively.

2.3.2 Measurement of cyclic water absorption capacity

1.0 g of dry carbon-based material was blended uniformly with 100 g of dry soil, and then placed in a ring knife with a filter paper lined at the bottom to prevent the mixture from leaking. Soil samples that had not been combined with biochar or carbon-based materials served as control subjects (labeled as control, CK). Afterwards, 150 mL of distilled water was added to the sample and left to saturate for 12 h. After achieving saturation, the moistened soil sample was then dried at 60 °C until reaching a consistent weight. For the mixed soil sample, an additional 150 mL of distilled water was consistently poured and left to saturate once more for 12 h span, prior to the sample being weighed again. This process of swelling, drying, and soaking was repeated five times to determine the reversibility of the carbon-based material and its water reabsorption capabilities. Each treatment was performed in triplicate. Finally, the circulating water absorption capacity (SR) was calculated using Eq. (3).

2.3.3 Infiltration experiment of carbon-based material in sandy soil

A one-dimensional fixed water head vertical ponding infiltration method was employed to evaluate the influence of carbon-based materials on soil infiltration. The infiltration setup comprised of a soil column and a Mariotte bottle, and

the soil column was a transparent Plexiglas cylinder, 10 cm in diameter and 45 cm in height. To prevent soil particles from escaping and to ensure aeration within the column, 1.0 cm of quartz sand and two layers of filter paper were placed at the base of the column. A thin layer of petroleum jelly was used to coat the pipe walls of the cylinder to lessen any effect of pipe wall effect on infiltration of water.

The experiment included the following five treatments: CK, BC, SB, SAB, and CB. The filling height of each soil column was 40 cm. BC and carbon-based materials were filled in the soil columns between 0–20 cm in amounts equivalent to 0.5% and 1.0% of the weight of 0–20 cm soil layer. The filling density was maintained at 1.4 g cm^{-3} , as per the soil bulk density observed in the field, and the soil was mixed thoroughly to ensure uniformity. We carefully filled the layers at 5 cm intervals, and made sure the layers were closely packed to avoid any stratification during the test. A Mariotte bottle with an inner diameter of 10 cm and a height of 50 cm was used to provide water to each column, with a water head of 25 mm (Additional file 1: Fig. S1). After infiltrating, vertical wetting peak's height of movement in the soil column and descent distance of water level in the Mariotte bottle were recorded continuously over a specific time period. The recording intervals were set as follows: every 2 min for the first 0 to 10 min, every 5 min from 10 to 60 min, every 10 min from 60 to 120 min, every 30 min from 120 to 420 min, every 60 min from 420 to 960 min, and then every 120 min for the remaining time. The recording ceased when the wetting peak reached the base. Water was supplied until the column was saturated and then soil samples were taken at 5 cm intervals from different layers for drying method analysis of the water content in the soil mass. Each treatment was performed in triplicate.

The power function (Ning et al. 2019) was employed to describe the dynamic process of the transport time and height of the wetting peak, which was simulated using Eq. (4).

$$F = at^b, \quad (4)$$

where F is the wetting peak transport distance, cm. t represents the infiltration time. a and b are empirical constants, a represents the wetting peak transport distance in the first time period after the start of infiltration, and b represents the decay of the wetting peak transport process.

The Philip model (Zhang et al. 2022) was used to simulate the infiltration process for different treatments, using Eq. (5).

$$I(t) = St^{0.5}, \quad (5)$$

where $I(t)$ is the cumulative infiltration, mm. S is the soil permeability rate, $\text{mm min}^{-0.5}$, and t is the infiltration time, min.

2.3.4 Measurement of water retention capacity of carbon-based materials in sandy soils

PVC columns, each with an inner diameter of 10 cm and a height of 45 cm, were selected for the test setup and soil filling. These sequences were consistent with those adopted in Sect. 2.3.3 Subsequently, all soil columns were filled with water to saturation and positioned in a reasonably steady indoor circumstance to enable natural evaporation. An electronic scale (Precision, 0.20 g) was used to weigh the columns on a weekly basis and the weight of each column was noted for a period of 91 days. Each treatment was replicated three times. Finally, Eq. (6) was worked through for computing the water retention rate of the soil.

$$\text{Water Retention (\%)} = \frac{W_t - W}{W_i - W} \times 100, \tag{6}$$

where W is the weight of the dry soil column, W_i is the weight of the soil column after water saturation, and W_t is the weight of the soil column after the specified time intervals.

2.3.5 Experimental evaluation of carbon-based materials on soybean germination

For this experiment, we used pots as germination platform, with soybeans as germinating plants. Five hundred g of sandy soil was added to each pot (10 cm × 10 cm × 9.0 cm), and 5.0 g of BC, SB, SAB, and CB were each thoroughly mixed into the sandy soil. Prior to planting, we disinfected the soybeans with 3.0% sodium hypochlorite for 5 min, then rinsed them three times with distilled water, planting one soybean plant per pot. The greenhouse conditions were a constant temperature of 25 °C an air humidity of 38%. The experimental design consisted of five treatments, i.e., Control (CK), BC, SB, SAB, and CB, with three replicate groups. Initial irrigation was set to 40 wt% of the soil. After 10 days, plant height was determined, separately.

2.3.6 Measurement of carbon-based materials affecting sandy soil aggregates

After natural evaporation in Sect. 2.3.4, soil samples were taken at 10 cm intervals, gently broken along the natural plane, air-dried at room temperature, and 50 g of aggregates of <5.0 mm were collected and weighed. Subsequently, these soil aggregates were determined by wet-sieving with a Soil Aggregate Analyzer (QT-WSI021, Beijing Channel Scientific Instruments Co., Ltd.). The Analyzer was shaken up and down in water at a frequency

of 30 times min^{-1} for 30 min. After sieving, the residual aggregates on each sieve were collected, dried and weighed and separated into six particle sizes: >2.0 mm, 2.0–1.0 mm, 1.0–0.5 mm, 0.5–0.25 mm, 0.25–0.106 mm, and <0.106 mm. Each treatment was replicated three times. Finally, the mean weight diameter (MWD) and the geometric mean diameter (GMD) were used for aggregate analysis, which were calculated by Eqs. (7) and (8) (Yang and Lu 2021).

$$\text{MWD} = \frac{\sum_{i=1}^6 m_i d_i}{\sum_{i=1}^6 m_i}, \tag{7}$$

$$\text{GMD} = \frac{\sum_{i=1}^6 m_i \ln \bar{d}_i}{\sum_{i=1}^6 m_i}, \tag{8}$$

where m_i is the mass of aggregate fraction i (g), and d_i is the mean diameter of the aggregate fraction i (mm).

2.4 Data processing and analysis

All experimental data were processed using Excel 2021 software (Microsoft Corp Redmond, USA). Origin 2018 software (OriginLab Corp., Northampton, USA) was employed for graphing. All statistical analyses were executed using IBM SPSS 26.0 software (IBM Corp., Armonk, NY, USA). One-way ANOVA was used to compare the differences among various treatments, and the significance level was set at $p < 0.05$.

3 Results

3.1 Characterization and analysis of materials

3.1.1 Grafting effect

AA was successfully grafted onto the structural backbone of starch, sodium alginate, and chitosan, and grafted onto the surface of BC employing MBA as crosslinker. MBA effectively formed a durable polymerization network in each polymer, contributing to the retention of moisture inside the polymerization link. Table 1 reveals that the G% and E% of CB were the most advantageous, suggesting that the grafting of AA and sodium alginate

Table 1 Comparison of grafting rate (G%) and grafting efficiency (E%) of starch-carbon-based material (SB), sodium alginate-carbon-based material (SAB) and chitosan-carbon-based material (CB)

Materials	G%	E%
SB	2107 ± 4.6c	64 ± 1.4a
SAB	2345 ± 17b	64 ± 1.2a
CB	2383 ± 6.3a	74 ± 1.8b

Different lowercase letters in the same column indicate significant differences ($p < 0.05$, LSD test)

onto the BC carrier was less difficult compared to SB and SAB. Nevertheless, SB and SAB demonstrated effective crosslinking grafting, with G% over 2000% and E% over 60%.

3.1.2 SEM analysis

Figure 2a, b highlight the distinct porosity and scattered pattern of BC. Figure 2c reveals that SB was strongly bound with starch, fully encapsulated by the enclosing amylose layer. Figure 2d presents a porous structure of the surface, displaying a heavily interconnected and visible pore structure, which improved the swelling rate of SB owing to the increased surface area it provided, and water absorption channels/sites, thus magnifying its water absorption capacity.

In comparison with the distributed BC, a small part of small and porous biochar aggregated when encased in sodium alginate, suggesting a satisfactory binding between the sodium alginate and AA monomer, and sodium alginate on the biochar's surface (Fig. 2e). The biochar maintained the original porous nature and formed a smoother layer, which diminished the hydrogen bonding interactions between hydrophilic groups such as hydroxyl and carboxyl groups in SAB, allowing more

hydrophilic functional groups to exist independently, further contributing to the absorption of water (Fig. 2f).

Figure 2g reveals that the biochar embedded within the chitosan retained its original porous structure, preserving its original characteristics, with a bumpy and uneven surface that increases its specific surface area, providing more sites for water molecules to attach and be retained.

3.1.3 Elemental analysis of carbon-based materials

After grafting polymerization of BC, the O and H contents of the resulting SB, SAB, and CB significantly increased (Table 2). The O/C ratios of SB, SAB, and CB were 11, 10, and 11 times higher than that of BC, while the H/C ratios also significantly exceeded that of BC. This suggests that SB, SAB, and CB possessed more oxygen-containing and hydrophilic functional groups than BC, thus significantly improving the hydrophilicity and polarity of BC (Wang et al. 2015). Moreover, the successful grafting of starch, sodium alginate and chitosan onto BC was also confirmed.

3.1.4 FT-IR analysis

The FT-IR of BC with peaks at 3422 cm⁻¹ presented peaks mainly representing the stretching vibrations of hydroxyl-OH and free carboxylic acid-OH, 2922 cm⁻¹

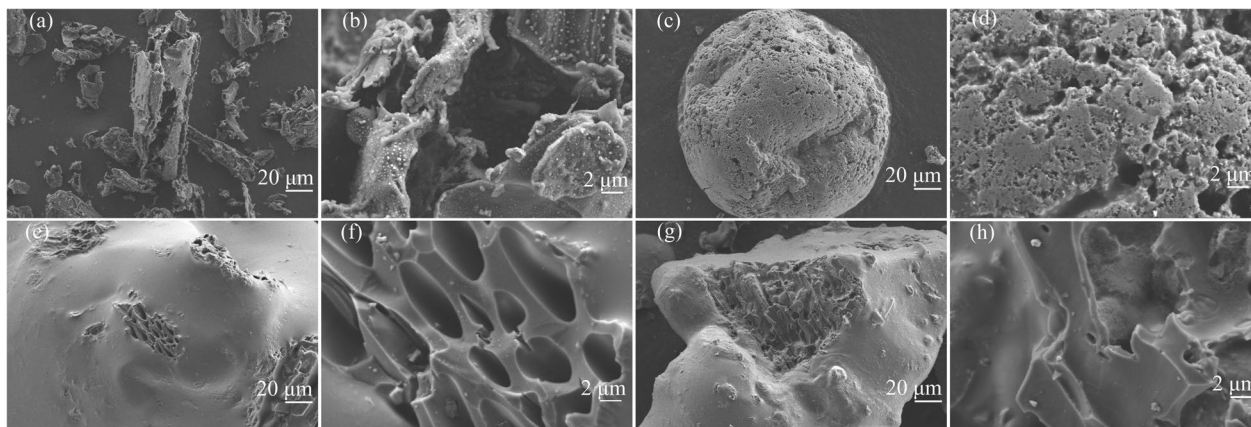


Fig. 2 SEM diagram of biochar (BC) (a, b), starch-carbon-based material (SB) (c and d), sodium alginate-carbon-based material (SAB) (e, f) and chitosan-carbon-based material (CB) (g, h)

Table 2 Physicochemical properties of biochar (BC), starch-carbon-based material (SB), sodium alginate-carbon-based material (SAB) and chitosan-carbon-based material (CB)

Materials	C (%)	N (%)	O (%)	H (%)	O/C	(O+N)/C	H/C
BC	74.25 ± 0.52a	1.11 ± 0.03a	12.09 ± 0.11d	1.86 ± 0.03d	0.12 ± 0.01d	0.13 ± 0.01c	0.30 ± 0.01d
SB	28.54 ± 0.27d	0.36 ± 0.01d	50.39 ± 0.79a	4.94 ± 0.04a	1.32 ± 0.02b	1.34 ± 0.02a	2.08 ± 0.04a
SAB	31.08 ± 0.34c	0.49 ± 0.01c	49.12 ± 0.40b	4.64 ± 0.04b	1.19 ± 0.02c	1.20 ± 0.01b	1.79 ± 0.01b
CB	32.96 ± 0.58b	0.52 ± 0.00b	45.98 ± 0.55c	4.34 ± 0.08d	1.39 ± 0.04a	1.11 ± 0.02d	1.58 ± 0.03c

Different lowercase letters in the same column indicate significant differences ($p < 0.05$, LSD test)

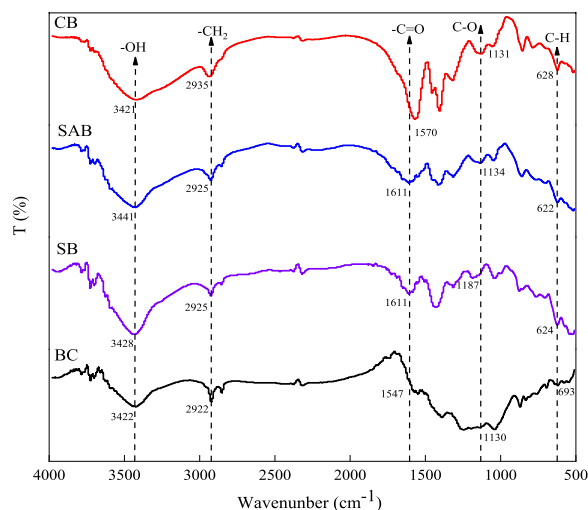


Fig. 3 FT-IR spectra of biochar (BC), starch-carbon-based material (SB), sodium alginate-carbon-based material (SAB) and chitosan-carbon-based material (CB)

had peaks mainly from the symmetric and asymmetric C–H stretching of CH_x groups of alkane compounds, and 1547 cm⁻¹ features prominently the free carboxylic acid C=O stretching vibrations (Fig. 3) (Tan et al. 2019). The characteristic peaks at 1390, 1245, and 1040 cm⁻¹ were dominantly C–O and O–H stretching vibrations, which disappeared after graft polymerization, indicating the involvement of C–OH in BC in the chemical reaction (Meng and Ye 2017). The characteristic peaks at 693 cm⁻¹ could come from monocyclic and polycyclic aromatic groups (Yao et al. 2011), primarily derived from C–H bending vibrations, showing that BC contains polar groups that can interact strongly with substances such as starch, sodium alginate, chitosan, and AA monomers via hydrogen bond formation. As Fig. 3 illustrates, the absorption bands of hydroxyl and carboxyl groups overlapped in the range of 3400–3600 cm⁻¹ and showed broad peaks in the three carbon-based materials (i.e., SB, SAB, and CB). The occurrence of peaks near 2920 cm⁻¹ for the three carbon-based materials might be associated with the extension of the –CH₂ group in AA (Baki and Abedi-Koupai 2018). Moreover, the distinctive peaks close to 1600 cm⁻¹ for the three carbon-based materials were mainly attributed to –COOH stretching vibrations, indicating the inclusion of AA in the grafted polymer, and the characteristic peaks near 1420 cm⁻¹ ascribed to the –CH₂ symmetric bending of BC indicated the presence of biochar within the carbon-based materials with new characteristic peaks near 620, 1600, and 1150 cm⁻¹ (Gao et al. 2023). The appearance of broad peaks in the three carbon-based materials further confirms the

successful grafting of starch, sodium alginate, and chitosan onto biochar through graft polymerization.

3.1.5 Contact angle

The hydrophilic nature of the substances was assessed using their respective contact angles. This study investigated the contact angles of BC, SB, SAB, and CB when interacting with water. As Fig. 4 demonstrates, the contact angle for BC was found to be 91.4°, while the contact angles for SB, SAB, and CB were 55.0°, 51.4°, and 42.6°, respectively. It is noteworthy that SB, SAB, and CB exhibited a greater degree of hydrophilicity compared to BC, but BC exhibited strong hydrophobicity.

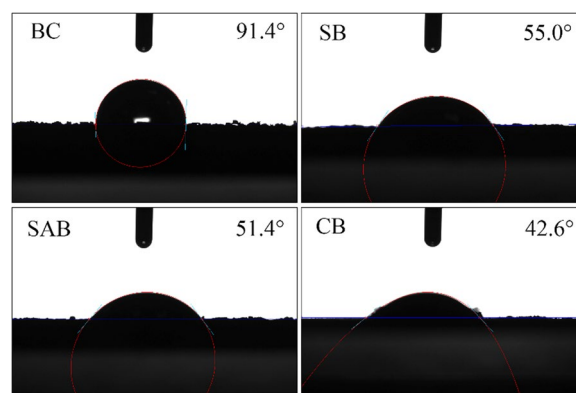


Fig. 4 Contact angle of biochar (BC), starch-carbon-based material (SB), sodium alginate-carbon-based material (SAB) and chitosan-carbon-based material (CB)

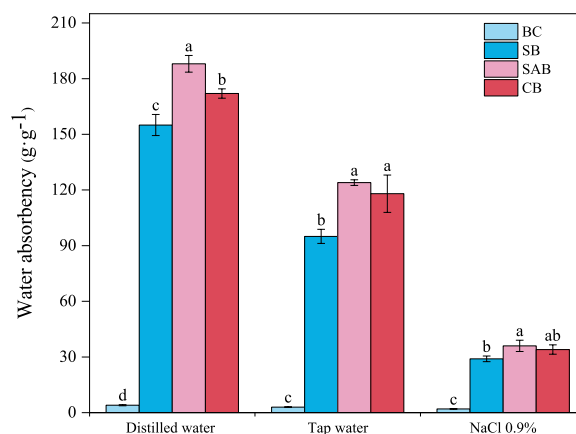


Fig. 5 Water absorption capacity of starch-carbon-based material (SB), sodium alginate-carbon-based material (SAB) and chitosan-carbon-based material (CB) in different solutions. Error bars indicate standard deviation; different lowercase letters indicate significant differences between the treatments ($p < 0.05$, LSD test) for different carbon-based materials in the same solution

3.2 Water absorption capacity of carbon-based materials

3.2.1 Water absorption capacity in different solutions

Figure 5 shows the effect of solutions with different ionic concentrations on the water absorption capacities of BC, SB, SAB, and CB. These four materials displayed different water absorption rates in different solutions. Specifically, their water absorption multiplicities were 4.0, 155, 188, and 172 g g⁻¹ for BC, SB, SAB, and CB in distilled water, 3.0, 95, 124, and 118 g g⁻¹ in tap water, and 2.0, 29, 36, and 34 g g⁻¹ in a 0.9 wt% NaCl solution.

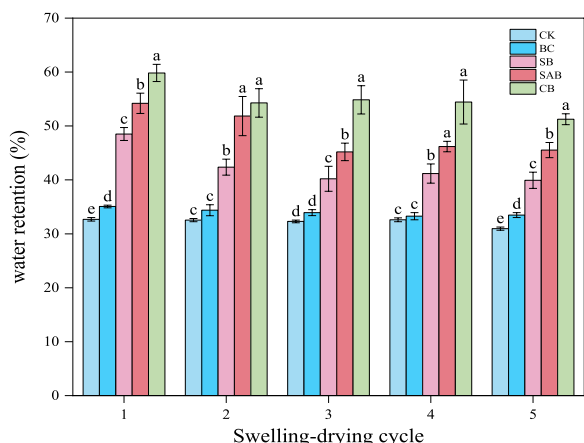


Fig. 6 Cyclic water absorption capacity of control (CK), biochar (BC), starch-carbon-based material (SB), sodium alginate-carbon-based material (SAB) and chitosan-carbon-based material (CB) in sandy soil. Error bars indicate standard deviation; different lowercase letters indicate significant differences between the treatments ($p < 0.05$, LSD test) for different carbon-based materials in the same cycle

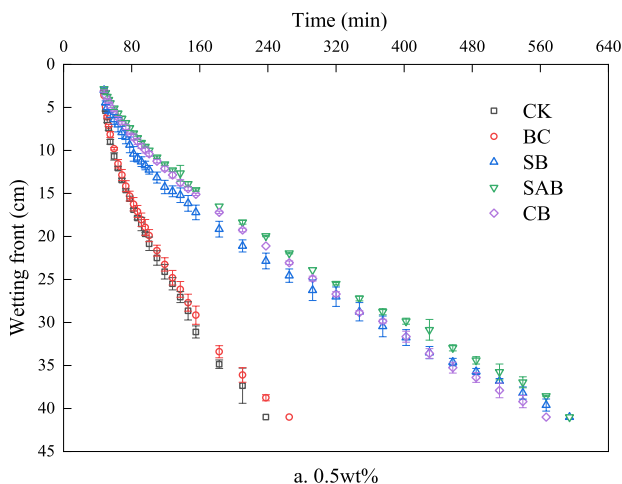
3.2.2 Water absorption capacity in sandy soils

The cyclic water absorption capacity of carbon-based materials in soil was profoundly significant for its practical application. Figure 6 reveals that BC, SB, SAB, and CB can sustain five cycles of swelling-drying water absorption in sandy soils, indicating that SB, SAB, and CB could potentially be recycled in such soils. After each drying cycle, the sandy soil amended with SB, SAB, and CB demonstrated an ability to absorb and retain water successively. After the fifth cycle, the water retention capacity of SB, SAB, and CB remained at 39%, 46%, and 51%, respectively. This was 8.0%, 15%, and 20% higher than that of CK. On the other hand, CK showed no significant difference in water retention capacity when compared to CK, with only 1.0% increase in the sandy soil's water retention capacity. Notably, the carbon-based material achieved peak water retention capacity during the first cycle, and thereafter gradually declined with each successive absorption cycle.

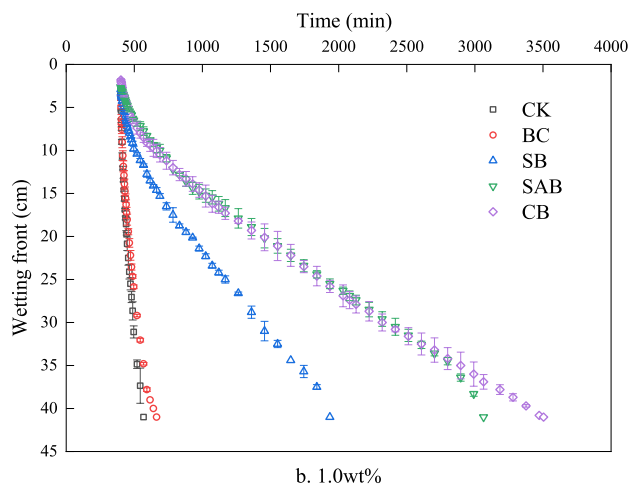
3.3 Effect of carbon-based materials on water infiltration in sandy soils

3.3.1 Impact on moisture peak transport

Figure 7 illustrates the impact of carbon-based materials on the dynamic process of soil wetting peaks at various addition ratios. The depth of wetting peak transport increased with infiltration time, leading to substantial differences in the time needed to reach a depth of 40 cm in the soil for different treatments. For 0.5 wt% of addition rates, CK, BC, SB, SAB, and CB required 210, 240, 600, 600, and 570 min, respectively. Compared to CK, BC did not significantly alter the infiltration dynamics, while SB, SAB, and CB prolonged the infiltration time by 185%, 185%, and 171%, respectively. At 1.0 wt% of addition, CK,



a. 0.5wt%



b. 1.0wt%

Fig. 7 Dynamic change of soil wetting peaks treated with control (CK), biochar (BC), starch-carbon-based material (SB), sodium alginate-carbon-based material (SAB) and chitosan-carbon-based material (CB) at different application rates. Error bars indicate standard deviation

BC, SB, SAB, and CB required 210, 330, 1920, 3330, and 3880 min, respectively. Compared to CK, BC, SB, SAB, and CB extended the infiltration time by 47%, 814%, 1485%, and 1509%, respectively. These findings reveal that the addition of SB, SAB, and CB to sandy soils can hamper the water penetration to deeper soil levels, thus increasing the soil's water content duration and improving water holding in sandy soils. Additionally, although BC did not have a pronounced effect on delaying water infiltration in comparison to SB, SAB, and CB, its influence on water infiltration in sandy soils can be recognized as the rate of addition increases.

Table 3 presents the fitting of the wetting peak versus infiltration time, indicating that the power function successfully modeled the wetting peak transport pattern of BC and the three carbon-based material treatments in sandy soil, with a coefficient of determination (R^2) greater than 0.98 for each treatment. Parameter a demonstrated a trend of $SAB < CB < SB < BC < CK$ for both 0.5 wt% and 1.0 wt% of addition ratio, which initially decreased and subsequently increased. Additionally, the interval of wet

peak transport of the fitted parameter power index b for each treatment did not present a clear pattern. Both parameters a and b demonstrate that different materials and levels of additions can visibly impact the initial moisture infiltration process dominated by the substrate potential.

3.3.2 Impact on cumulative infiltration

The cumulative infiltration of soil water naturally increased over time, with each treatment group affecting this process distinctly. The cumulative infiltration of SB decreased as the addition ratio increased, whereas the cumulative infiltration of BC, SAB, and CB increased with an increase in the addition ratio. All four materials enhanced the cumulative infiltration of the soil, with CB resulting in the highest cumulative infiltration (Fig. 8). In comparison with CK, the cumulative infiltration of SB, SAB, and CB was notably higher in the 0.5 wt% addition group, increasing by 15%, 13%, and 11%, respectively. Moreover, the cumulative infiltration of the three carbon-based materials did not show significant differences

Table 3 Effects of biochar (BC), starch-carbon-based material (SB), sodium alginate-carbon-based material (SAB) and chitosan-carbon-based material (CB) on soil infiltration

Treatments	0.5 wt%			1.0 wt%		
	a	b	R^2	a	b	R^2
CK	2.42 ± 0.01a	0.52 ± 0.00b	0.99	2.42 ± 0.01a	0.53 ± 0.00b	0.99
BC	2.38 ± 0.14a	0.52 ± 0.01b	0.99	2.41 ± 0.15a	0.50 ± 0.01c	0.99
SB	1.46 ± 0.13b	0.51 ± 0.01b	0.99	0.80 ± 0.03b	0.51 ± 0.01c	0.98
SAB	0.85 ± 0.02c	0.59 ± 0.00a	0.99	0.35 ± 0.01c	0.58 ± 0.00a	0.98
CB	0.91 ± 0.01c	0.59 ± 0.00a	0.99	0.40 ± 0.04c	0.56 ± 0.01a	0.99

Different lowercase letters in the same column indicate significant differences ($p < 0.05$, LSD test)

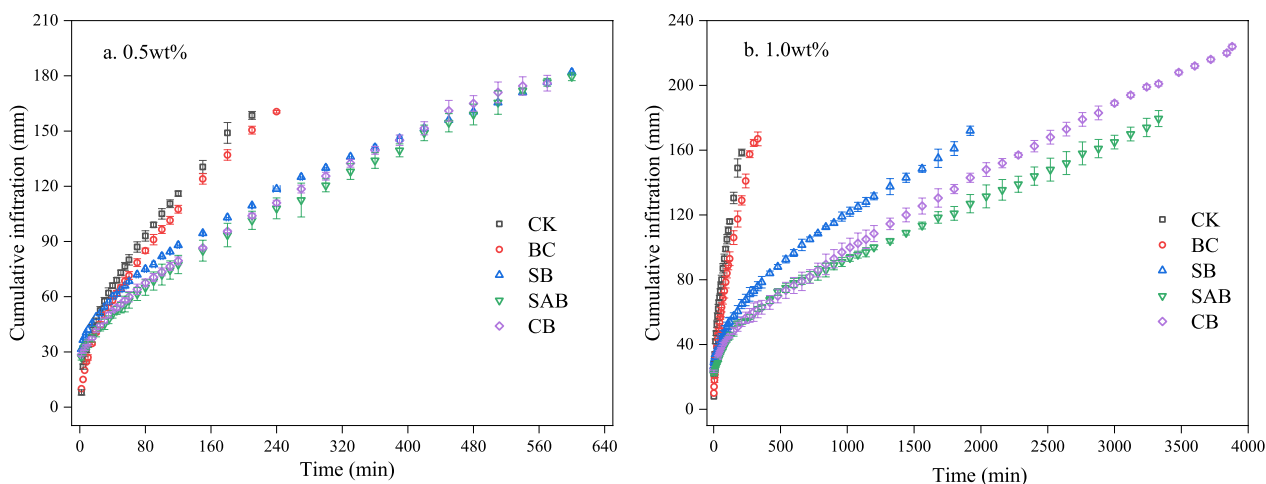


Fig. 8 Effects of control (CK), biochar (BC), starch-carbon-based material (SB), sodium alginate-carbon-based material (SAB) and chitosan-carbon-based material (CB) on soil cumulative infiltration under different application rates. Error bars indicate standard deviation

along with the increase of infiltration time. In contrast, the cumulative infiltration of BC in the same group had no obvious change compared to the CK. However, at 1.0 wt% addition rate, there was a significant difference in the effect of SB, SAB, and CB on cumulative infiltration. CB demonstrated the largest cumulative infiltration, showing a 41% increase compared to CK. SB and SAB increased by 10% and 13% compared to CK, respectively. Meanwhile, BC at 1.0 wt% addition rate showed an increase of 5.0% in cumulative infiltration relative to CK throughout the entire cumulative infiltration process.

The coefficients of determination (R^2) for the Philip model with cumulative infiltration fitted all exceeded 0.93 (Table 4), indicating that the application of BC and the three carbon-based materials to the 0–20 cm soil layer of the sandy soil could bring about a good fit for the simulated water infiltration. Moreover, the soil permeability rate S suggested that the addition of SB, SAB, and

CB significantly decreased the sandy soil’s permeability capacity and infiltration capacity ($p < 0.05$).

3.3.3 Impact on the water content of different infiltrated soil layers

For all the treatments, the soil water content decreased with increasing soil depth and remained relatively constant (Fig. 9). When 0.5 wt% SB, SAB, and CB were added, the water content in the 0–5 cm soil layer significantly increased by 8.0%, 9.0%, and 8.0%, respectively compared to the CK, and the 6–10 cm soil layer increased by 6.0%, 8.0%, and 6.0% compared to CK, respectively. Furthermore, the water content of the remaining soil layers stayed approximately at 22%, the same as in the CK. When 1.0 wt% of the three carbon-based materials was applied, the water content also significantly increased, with SB, SAB, and CB treatments producing a 15%, 20%, and 20% soil content increase in the 0–5 cm soil layer when compared to CK, respectively, 9.0%, 18%, and 15% water content increase in the 6–10 cm soil layer compared to CK, respectively. The addition of SAB most significantly increased the infiltration water content, while neither 0.5 wt% nor 1.0 wt% BC exerted a significant effect on the water content of the soil.

Table 4 Philip infiltration model fitting parameters of biochar (BC), starch-carbon-based material (SB), sodium alginate-carbon-based material (SAB) and chitosan-carbon-based material (CB)

Treatments	0.5 wt%		1.0 wt%	
	S	R^2	S	R^2
CK	10.62 ± 1.65a	0.99	10.62 ± 1.65a	0.99
BC	9.80 ± 0.13a	0.99	8.81 ± 0.53b	0.98
SB	7.46 ± 0.04ab	0.95	3.96 ± 0.07c	0.93
SAB	7.26 ± 0.21b	0.98	3.03 ± 0.10c	0.96
CB	7.46 ± 0.13ab	0.98	3.39 ± 0.10c	0.98

Different lowercase letters in the same column indicate significant differences ($p < 0.05$, LSD test)

3.4 Effect of carbon-based materials on soil water retention capacity

The water-holding capacity of soil is vital for assessing the potential of SB, SAB, and CB as soil conditioners. Figure 10 shows the variation of water retention rate of soil in different treatments with different additions in 91 days. The results showed that the soil columns with

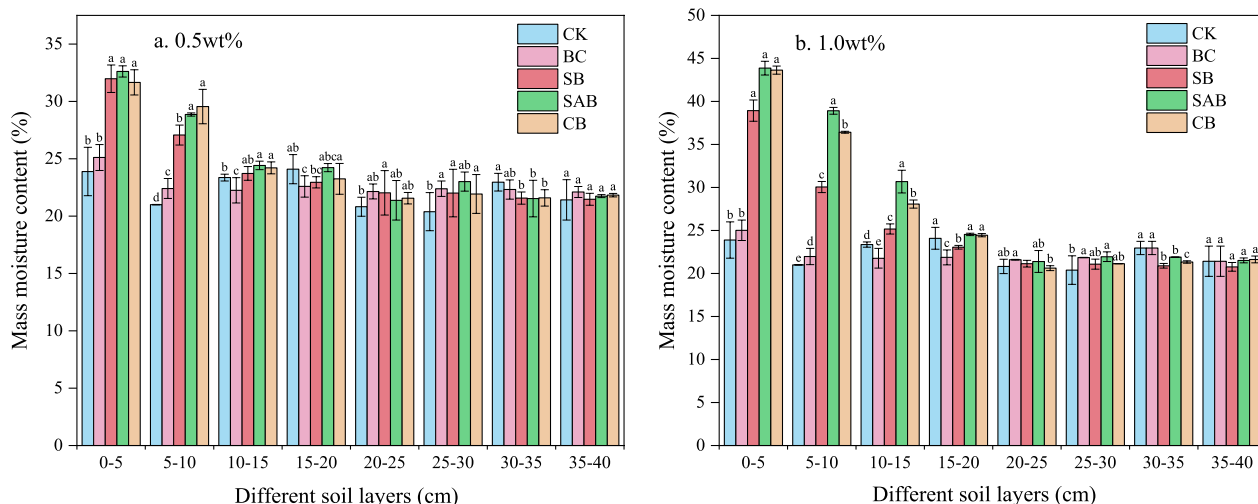


Fig. 9 Effects of control (CK), biochar (BC), starch-carbon-based material (SB), sodium alginate-carbon-based material (SAB) and chitosan-carbon-based material (CB) on soil water content distribution under different application rates. Error bars indicate standard deviation; different lowercase letters indicate significant differences between different carbon-based materials in the same soil layer ($p < 0.05$, LSD test)

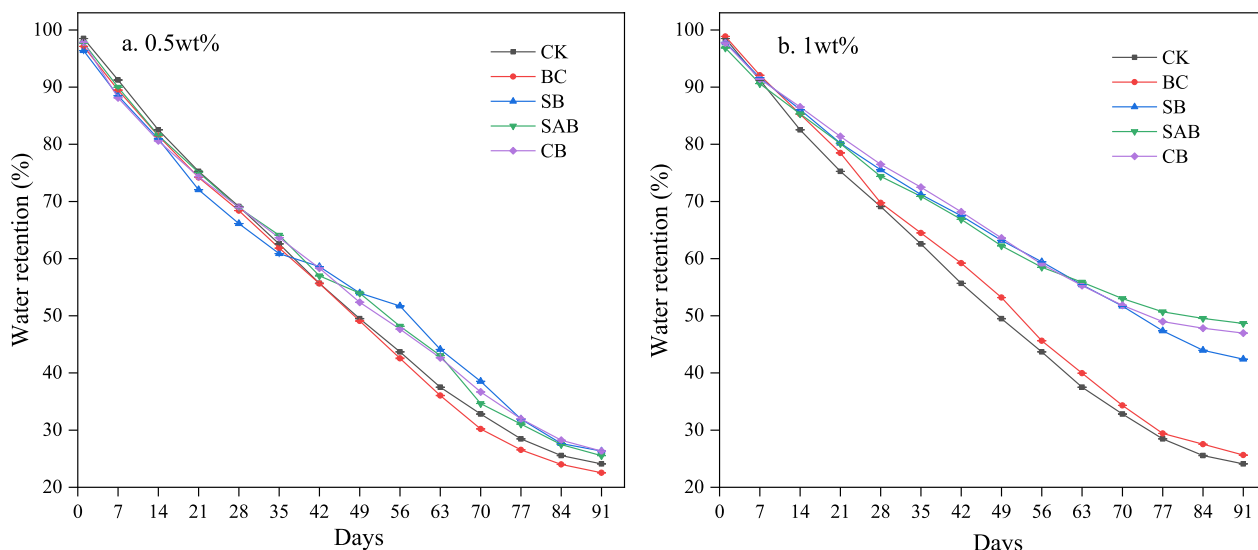


Fig. 10 Control (CK), biochar (BC), starch-carbon-based material (SB), sodium alginate-carbon-based material (SAB) and chitosan-carbon-based material (CB) at different application rates and their effects on soil water retaining capacity. Error bars indicate standard deviation

the three carbon-based materials added had higher water retention. For an addition of 0.5 wt%, the water retention rate of SB, SAB, and CB increased by 2.0%, 1.0%, and 2.0% respectively when compared to the control (CK) whereas the water retention rate of BC treatment dropped by 2.0% in comparison with CK. With a 1.0 wt% addition, water retention increased by 18%, 25%, and 23% for SB, SAB, and CB, respectively, relative to CK, while the increase for the BC treatment was 2.0%.

Figure 11 demonstrates the significant influence of BC, SB, SAB, and CB on plant height and root growth when sowed in sandy soil for soybean germination. After 10 days of incubation, the plant heights of CK, BC, SB,

SAB, and CB were 8.20 ± 0.24 , 15.90 ± 0.69 , 15.90 ± 0.81 , 19.00 ± 0.65 , and 16.50 ± 0.49 cm, and the plant heights of BC, SB, SAB, and CB treatments were significantly increased by 7.70, 7.70, 10.80, and 8.30 cm compared with CK. Furthermore, the primary roots of plants applied with SB, SAB and CB were noticeably thicker, with additional lateral root growth.

3.5 Effect of carbon-based materials on the size distribution and stability of soil aggregates

The use of three carbon-based materials (i.e., SB, SAB, and CB) affected the distribution of the various-sized aggregates in different soil layers (Additional file 1: Figs.



Fig. 11 Effect of control (CK), biochar (BC), starch-carbon-based material (SB), sodium alginate-carbon-based material (SAB) and chitosan-carbon-based material (CB) on plant germination

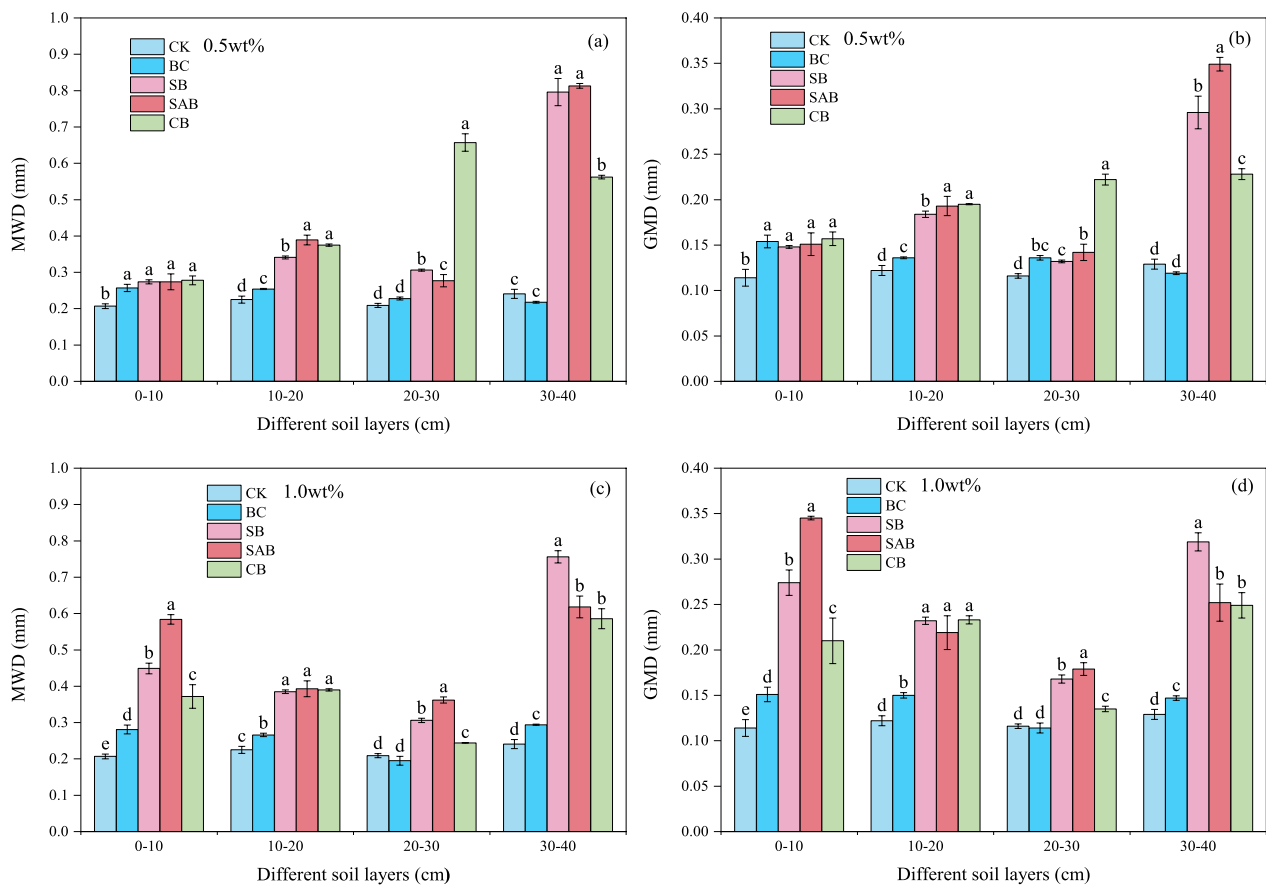


Fig. 12 Effects of control (CK), biochar (BC), starch-carbon-based material (SB), sodium alginate-carbon-based material (SAB) and chitosan-carbon-based material (CB) on aggregate stability in different soil layers under different application rates. Error bars indicate standard deviation; different lowercase letters indicate significant differences between the treatments ($p < 0.05$, LSD test) for different carbon-based materials in the same soil layer

S2, S3), which tended to increase and then decrease as the soil layer’s depth increased. It was also apparent that the carbon-based materials efficiently promoted the formation of aggregates ranging from 2.0 to 0.25 mm. Figure 12 reveals that the SB, SAB, and CB treatments resulted in a marked improvement in both the MWD and GMD of the aggregates, especially in the 30–40 cm soil layer. At a 0.5 wt% application rate, the MWD of SB, SAB, and CB had an increase of 0.56, 0.57, and 0.32 mm in the 30–40 cm soil layer, respectively, compared to CK (Fig. 12a), and the GMD increased by 0.17, 0.22, and 0.11 mm (Fig. 12b). At the application rate of 1.0 wt%, the MWD of SB, SAB, and CB increased by 0.52, 0.38, and 0.34 mm in the 30–40 cm soil layer, respectively, compared to CK (Fig. 12c), and the GMD of SB, SAB, and CB increased by 0.16, 0.21, and 0.10 mm in soil layers 0–10 cm compared to CK (Fig. 12d). Similarly, for a 1.0 wt% application rate, the BC treatment resulted in a decrease of the MWD and GMD in the 20–30 cm soil layer (Fig. 12). Nevertheless, in the other soil layers, the

enrichment in MWD and GMD by means of the BC treatment was not significant when compared to SB, SAB, and CB.

4 Discussion

4.1 Water absorption capacity of the carbon-based materials

This study found that SB, SAB, and CB presented excellent water absorption properties. However, significant differences were observed in their water absorption characteristics. This could potentially be due to the introduction of different amounts of BC, MBA, and AA, which leads to various levels of hydrophilic functional groups on the established polymer network. This has been confirmed by Rodrigues et al. (2012), who argued that the water retention materials create a higher density of crosslinking sites as the amount of MBA in the formation of polymers increases, rendering better structural stability and greater water retention. AA is the chief influencing factor in the water absorption of water retention

materials, bringing in more hydrophilic functional groups (–COOH and –OH) in the main and side chains of the formed polymer (Zhong et al. 2012). These functional groups, in combination with water, form water molecules between them and are adsorbed on the polymeric network of carbon-based water retention materials, increasing water absorption (Huang et al. 2022). The various water absorption ratios observed in the three solutions may be due to the fact that the water absorption capacity of carbon-based water retention materials was affected by the disparity in osmotic pressure inside and outside of the polymer network. This osmotic effect diminishes as ion concentration in the solution rises, leading to a decrease in water absorption capacity (Xu et al. 2015). Furthermore, the SB, SAB, and CB demonstrated salt tolerance, as indicated by their water absorption rates in 0.9 wt% NaCl solution. Additional file 1: Table S1 provides a comparative analysis of the water absorption capacities of the carbon-based materials under study, with results from other researchers. Compared with other carbon-based materials, the three carbon-based materials in this study have a higher water absorption capacity. This suggests that these materials can be utilized to improve sandy soils, and even saline sandy soils in extremely arid regions. Our study also found that the water absorption capacity of these materials declined progressively with the extension of the cycling period. This could be due to the degradation or alteration in the internal structure of the carbon-based material during the drying cycle in combination with the soil, where in each carbon-based material the particles were sheathed by soil particles in a specific setting and the swelling and water absorption capability of the carbon-based water holding material was limited, ultimately leading to a weakened water absorption capacity (Durpekova et al. 2021). Nevertheless, the remarkable cyclic water absorption capacity enhances the service life of SB, SAB, and CB, reducing costs and presenting promising prospects for the application of these materials.

4.2 Effect of carbon-based materials on soil infiltration

Soil infiltration process is influenced by its inherent characteristics. Sandy soils with their poor structure, low soil bulk, high porosity, and high hydraulic conductivity present unique challenges (Huang and Hartemink 2020). Carbon-based materials, when used as soil conditioners, will bring multiple hydrophilic functional groups of their own, which can alter the hydraulic properties of sandy soils. This study highlighted that the three carbon-based materials (i.e., SB, SAB, and CB) significantly prolonged the infiltration time of sandy soils, with their water-holding capacity notably exceeding that of biochar in sandy soils. The carbon-based materials introduced

more oxygen-containing functional groups and hydrophilic groups to biochar, thereby improving its hydrophilicity and polarity. When water infiltrates downwards, the carbon-based materials can bind with the soil particles to create flocculated soil, therefore raising the viscosity of the soil's liquid phase and enhancing its water retention effect.

In addition, the influence of carbon-based materials on the water infiltration rate in sandy soils is contingent on the application amount. With an application of 1.0 wt%, the infiltration time of SB, SAB, and CB carbon-based materials in sandy soils were significantly prolonged, reaching 1320, 2730, and 3310 min compared to the application of 0.5 wt%, possibly due to the carbon-based materials enabling the formation of a good surface texture in sandy soils. Furthermore, the maximum volumetric water content within the sandy soil escalates with the utilization of carbon-based material, consequently suppressing the infiltration of water into the sandy soil. The excess carbon-based material may block the interstices amongst the sandy soils when they absorb and swell, resulting in denser soil particle distribution. This situation slows the water infiltration through both the soil's interior pores and those of the carbon-based material, consequently lowering the rate of water infiltration (Zhao et al. 2019). The three carbon-based materials examined in this study markedly decelerated water infiltration in sandy soils at lower application rates. However, the biochar results indicated that, at low application rates, it instead facilitated water infiltration in sandy soils. Only at high application rates did it inhibit water infiltration, thereby enhancing the hydraulic properties of the sandy soils (Pu et al. 2019).

4.3 Water retention mechanism of carbon-based materials on sandy soil and plant

Seed germination and the seedling stage are critical phases in a plant's life cycle and are vital to establishing plant communities and improving stable, high-yield agricultural crops (Roberts and Ellis 1989). Soil moisture, one of the most crucial factors influencing plant seed germination and seedling growth, regulates seed germination and determines seedling survival (Baskin 2017; Lewandowski et al. 2021). In this study, we examined the impact of incorporating three carbon-based materials (i.e., SB, SAB, and CB) into sandy soil on soybean seed germination. Our findings revealed that the introduction of SB, SAB, and CB had positive effects on early-stage soybean growth. This can be attributed, firstly, to the water-adsorbing capability of carbon-based materials, enabling the sandy soil to retain larger volumes of water and release it gradually. Secondly, these carbon-based materials substances enhanced the sandy soil's water-holding

capacity, thus preserving more water in the soil. Concurrently, the soil's volume increased due to the water-absorption process of carbon-based materials, lowering the soil's bulk density. Consequently, more water became available to the plant roots, promoting their growth and development. Furthermore, as the soil contracted with the loss of water during plant growth, the soil's internal porosity improved, facilitating air circulation within the soil and thereby providing a conducive environment for plant growth (Eibisch et al. 2015). However, caution must be taken to avoid an excessive addition of carbon-based materials, as over-saturation could fill the soil's pores, causing undue soil expansion that could hinder crop root growth and diminish soil air permeability, potentially causing plant root hypoxia and adversely impacting plant growth (Guo et al. 2020).

On the other hand, soil aggregates play a pivotal role in enhancing soil fertility, promoting soil carbon absorption and stability. Our research indicated that carbon-based materials were more effective on coalescing sandy soil particles than biochar. This resulted in more robust formation of soil colloids, a larger number of soil aggregates, and the development of macroaggregates. As soil depth and application rate increased, these aggregates exhibited higher stability, ameliorating the sandy soil's physical structure and mechanical composition (Feng et al. 2020). This resulted in an augmented water-holding capacity, supplying more water for plant growth.

In summary, among the three carbon-based materials (i.e., SB, SAB, and CB), SB excelled in promoting aggregate formation and enhancing soil stability. CB, on the other hand, exhibited the strongest capability for soil water circulation and infiltration, contributing to the reduction of water infiltration in sandy soils. Meanwhile, SAB possessed better water absorption and retention capacities, making it the most effective in fostering plant growth. Therefore, for practical applications in sandy soil improvement, SAB should be the preferred choice over SB and CB.

5 Conclusions

This research has successfully pioneered the synthesis of three distinct carbon-based materials conducive to water retention: SB, SAB, and CB, employing the technique of graft polymerization. An exploration of the water absorption capacities of these materials was conducted, in conjunction with a study of their influence on the water retention attributes of sandy soils. Our analysis revealed that these materials substantially augmented the water absorption capacity of biochar. The three carbon-based materials also markedly prolonged infiltration times, concurrently amplifying the water retention capabilities of sandy soil, superseding the effects of solely incorporating

BC. Additionally, treatments involving SB, SAB, and CB stimulated the growth of soybean seedlings, dramatically improving sandy soil aggregates and enhancing their structural stability. In essence, SB, SAB, and CB showcased remarkable water absorption capacities and a modicum of salt resistance. They were capable of minimizing water infiltration in sandy soils, boosting the water retention capacity and augmenting the mechanical composition strength of these soils. This underlines the significant potential of SB, SAB, and CB in fortifying the water retention capacity and soil structure of semi-arid and arid sandy soils, thereby facilitating vegetation restoration and paving the way for potential large-scale deployment.

Supplementary Information

The online version contains supplementary material available at <https://doi.org/10.1007/s42773-023-00260-8>.

Additional file 1: Table S1: The water absorption of the carbon-based material in this paper is comparable to other paper. **Figure S1:** Schematic of soil water infiltration test. **Figure S2:** Effect of control (CK), biochar (BC), starch-carbon-based material (SB), sodium alginate-carbon-based material (SAB) and chitosan-carbon-based material (CB) on the particle size distribution of aggregates in different soil layers at 0.5% application rate. **Figure S3:** Effect of control (CK), biochar (BC), starch-carbon-based material (SB), sodium alginate-carbon-based material (SAB) and chitosan-carbon-based material (CB) on the particle size distribution of aggregates in different soil layers at 1.0% application rate.

Acknowledgements

The authors thank the valuable comments of anonymous reviewers and Editor.

Author contributions

YY: Experimental part, Data curation, Writing. FL: Conceptualization, Writing, Supervision, Funding acquisition. YY: Experimental part, Supervision. MZ: Discussion, Software. XB: Discussion, Software.

Funding

This research was supported by the Bingtuan Science and Technology Program (2021DB019; 2022CB001-01; 2022CB001-07), the National Natural Science Foundation of China (42275014).

Availability of data and materials

Data will be made availability on request.

Declarations

Ethical approval and consent to participate

Not applicable.

Consent for publication

Agree.

Competing interests

The authors declare no competing interests.

Author details

¹College of Water Resources and Architectural Engineering, Tarim University, Alar 843300, China. ²Key Laboratory of Tarim Oasis Agriculture (Tarim University), Ministry of Education, Alar 843300, China.

Received: 12 April 2023 Revised: 5 September 2023 Accepted: 9 September 2023

Published online: 27 September 2023

References

- Albalasmeh AA, Hamdan EH, Gharaibeh MA, El Hanandeh A (2021) Improving aggregate stability and hydraulic properties of sandy loam soil by applying polyacrylamide polymer. *Soil till Res* 206:104821
- Alghamdi AG, Alkhasha A, Ibrahim HM (2020) Effect of biochar particle size on water retention and availability in a sandy loam soil. *J Saudi Chem Soc* 24:1042–1050
- Baiamonte G, Crescimanno G, Parrino F, De Pasquale C (2019) Effect of biochar on the physical and structural properties of a sandy soil. *Catena (Amst)* 175:294–303
- Baki M, Abedi Koupai J (2018) Preparation and characterization of a superabsorbent slow-release fertilizer with sodium alginate and biochar. *J Appl Polym Sci* 135:45966
- Baskin CC (2017) Seed ecology: a diverse and vibrant field of study. *Seed Sci Res* 27:61–64
- Campos EVR, de Oliveira JL, Fraceto LF, Singh B (2015) Polysaccharides as safer release systems for agrochemicals. *Agron Sustain Dev* 35:47–66
- Chen X, Duan M, Zhou B, Cui L (2022) Effects of biochar nanoparticles as a soil amendment on the structure and hydraulic characteristics of a sandy loam soil. *Soil Use Manage* 38:836–849
- Chintala R, Schumacher TE, Kumar S, Malo DD, Rice JA, Bleakley B, Chilom G, Clay DE, Julson JL, Papiernik SK, Gu ZR (2014) Molecular characterization of biochars and their influence on microbiological properties of soil. *J Hazard Mater* 279:244–256
- Diao M, Li Q, Xiao H, Duan N, Xu J (2014) Synthesis and adsorption properties of superabsorbent hydrogel and peanut hull composite. *J Environ Chem Eng* 2:1558–1567
- Downie A, Crosky A, Munroe P (2012) Physical properties of biochar. *Biochar Environ Manag* 45–64
- Durpekova S, Di Martino A, Dusankova M, Drohlsler P, Sedlarik V (2021) Biopolymer hydrogel based on acid whey and cellulose derivatives for enhancement water retention capacity of soil and slow release of fertilizers. *Polymers (basel)* 13:3274
- Edeh IG, Mašek O (2022) The role of biochar particle size and hydrophobicity in improving soil hydraulic properties. *Eur J Soil Sci* 73:e13138
- Eibisch N, Durner W, Bechtold M, Fuß R, Mikutta R, Woche SK, Helfrich M (2015) Does water repellency of pyrochars and hydrochars counter their positive effects on soil hydraulic properties? *Geoderma* 245:31–39
- Feng W, Gao J, Cen R, Cen R, Yang F, He Z, Wu J, Miao Q, Liao H (2020) Effects of polyacrylamide-based super absorbent polymer and corn straw biochar on the arid and semi-arid salinized soil. *Agriculture* 10:519
- Gao L, Li Z, Yi W et al (2023) Effective Pb²⁺ adsorption by calcium alginate/modified cotton stalk biochar aerogel spheres: with application in actual wastewater. *J Environ Chem Eng* 11:109074
- Guilherme MR, Aouada FA, Fajardo AR, Martins AF, Paulino AT, Davi MFT, Rubira AF, Muniz EC (2015) Superabsorbent hydrogels based on polysaccharides for application in agriculture as soil conditioner and nutrient carrier: a review. *Eur Polym J* 72:365–385
- Guo J, Shi W, Wen L, Shi X, Li J (2020) Effects of a super-absorbent polymer derived from poly- γ -glutamic acid on water infiltration, field water capacity, soil evaporation, and soil water-stable aggregates. *Arch Agron Soil Sci* 66:1627–1638
- Hengl T, Mendes De Jesus J, Heuvelink GB (2017) Soilgrids250m: global gridded soil information based on machine learning. *PLoS ONE* 12:e169748
- Huang J, Hartemink AE (2020) Soil and environmental issues in sandy soils. *Earth Sci Rev* 208:103295
- Huang W, Lai H, Du J, Zhou C, Liu Z, Ni Q (2022) Effect of polymer water retaining agent on physical properties of silty clay. *Chem Biol Technol Agric* 9:1–13
- Iqbal S, Khan HZ, Li T, Arif M (2018) Organic nitrogen source addition for improving the physicochemical properties of sandy loam soil and maize performance. *Commun Soil Sci Plant Anal* 49:13–29
- Jilková V, Angst G (2022) Biochar and compost amendments to a coarse-textured temperate agricultural soil lead to nutrient leaching. *Appl Soil Ecol* 173:104393
- Lewandowski W, Stevens JC, Webber BL, Dalziel DL, Trudgen MS, Bateman AM, Erickson TE (2021) Global change impacts on arid zone ecosystems: seedling establishment processes are threatened by temperature and water stress. *Ecol Evol* 11:8071–8084
- Liu Z, Dugan B, Masiello CA, Barnes RT, Gallagher ME, Gonnermann H (2016) Impacts of biochar concentration and particle size on hydraulic conductivity and doc leaching of biochar–sand mixtures. *J Hydrol (amst)* 533:461–472
- Liu Z, Dugan B, Masiello CA, Gonnermann HM (2017) Biochar particle size, shape, and porosity act together to influence soil water properties. *PLoS ONE* 12:e179079
- Liu Y, Zhu Y, Mu B, Wang Y, Quan Z, Wang A (2021) Synthesis, characterization, and swelling behaviors of sodium carboxymethyl cellulose-g-poly (acrylic acid)/semi-coke superabsorbent. *Polym Bull (Berl)* 1–19
- Lv N, Lu H, Pan W, Meadows ME (2022) Factors controlling spatio-temporal variations of sandy deserts during the past 110 years in Xinjiang, North-western China. *J Arid Environ* 201:104749
- Mao J, Zhang K, Chen B (2019) Linking hydrophobicity of biochar to the water repellency and water holding capacity of biochar-amended soil. *Environ Pollut* 253:779–789
- Meng Y, Ye L (2017) Synthesis and swelling property of superabsorbent starch grafted with acrylic acid/2-acrylamido-2-methyl-1-propanesulfonic acid. *J Sci Food Agric* 97:3831–3840
- Ning S, Jumai H, Wang Q, Zhou B, Su L, Shan Y, Zhang J (2019) Comparison of the effects of polyacrylamide and sodium carboxymethylcellulose application on soil water infiltration in sandy loam soils. *Adv Polym Technol* 2019
- Noordin N, Jamari S, Ghazali S (2020) Swelling kinetic behavior of biochar-graft superabsorbent polymer composites. In: *IOP Conference Series: Materials Science and Engineering*. p 52029
- Parihar CM, Yadav MR, Jat SL, Singh AK, Kumar B, Pradhan S, Chakraborty D, Jat ML, Jat RK, Saharawat YS, Yadav OP (2016) Long term effect of conservation agriculture in maize rotations on total organic carbon, physical and biological properties of a sandy loam soil in north-western Indo-Gangetic plains. *Soil till Res* 161:116–128
- Phillips CL, Light SE, Gollany HT, Chiu S, Wanzek T, Trippe MK (2020) Can biochar conserve water in Oregon agricultural soils? *Soil till Res* 198:104525
- Pu S, Li G, Tang G, Zhang Y, Xu W, Feng G, Ding F (2019) Effects of biochar on water movement characteristics in sandy soil under drip irrigation. *J Arid Land* 11:740–753
- Roberts EH, Ellis RH (1989) Water and seed survival. *Ann Bot* 63:39
- Rodrigues FH, Fajardo AR, Pereira AG, Ricardo NM, Feitosa J, Muniz EC (2012) Chitosan-graft-poly (acrylic acid)/rice husk ash based superabsorbent hydrogel composite: preparation and characterization. *J Polym Res* 19:1–10
- Sutradhar SC, Khan MMR, Rahman MM, Dafadar NC (2015) The synthesis of superabsorbent polymers from a carboxymethylcellulose/acrylic acid blend using gamma radiation and its application in agriculture. *J Phys Sci* 26:23
- Tan G, Liu Y, Xiao D (2019) Preparation of manganese oxides coated porous carbon and its application for lead ion removal. *Carbohydr Polym* 219:306–315
- Verheijen FG, Zhuravel A, Silva FC, Amaro A, Ben-Hur M, Keizer JJ (2019) The influence of biochar particle size and concentration on bulk density and maximum water holding capacity of sandy vs sandy loam soil in a column experiment. *Geoderma* 347:194–202
- Wang S, Gao B, Li Y, Mosa A, Zimmerman AR, Ma L, Harris WQ, Migliacchi KW (2015) Manganese oxide-modified biochars: preparation, characterization, and sorption of arsenate and lead. *Bioresour Technol* 181:13–17
- Wang W, Yang Z, Zhang A, Yang S (2021) Water retention and fertilizer slow release integrated superabsorbent synthesized from millet straw and applied in agriculture. *Ind Crops Prod* 160:113126
- Weber K, Quicker P (2018) Properties of biochar. *Fuel (Lond)* 217:240–261
- Wiersma W, van der Ploeg MJ, Sauren IJ, Stoof CR (2020) No effect of pyrolysis temperature and feedstock type on hydraulic properties of biochar and amended sandy soil. *Geoderma* 364:114209

- Xi J, Zhang P (2021) Application of super absorbent polymer in the research of water-retaining and slow-release fertilizer IOP Conference Series. Earth Environ Sci p 42066
- Xu X, Bai B, Ding C, Wang H, Suo Y (2015) Synthesis and properties of an ecofriendly superabsorbent composite by grafting the poly (acrylic acid) onto the surface of dopamine-coated sea buckthorn branches. *Ind Eng Chem Res* 54:3268–3278
- Yang CD, Lu SG (2021) Effects of five different biochars on aggregation, water retention and mechanical properties of paddy soil: a field experiment of three-season crops. *Soil Till Res* 205:104798
- Yao Y, Gao B, Inyang M, Zimmerman AR, Cao X, Pullammanappallil P, Yan L (2011) Biochar derived from anaerobically digested sugar beet tailings: characterization and phosphate removal potential. *Bioresour Technol* 102:6273–6278
- Yu X, Lei J, Gao X (2022) An over review of desertification in Xinjiang, Northwest China. *J Arid Land* 1–15
- Zhang L, Jing Y, Chen G, Wang X, Zhang R (2019) Improvement of physical and hydraulic properties of desert soil with amendment of different biochars. *J Soils Sediments* 19:2984–2996
- Zhang Y, Zhen Q, Cui Y, Zhang P, Zhang X (2020) Use of montmorillonite-enriched siltstone for improving water condition and plant growth in sandy soil. *Ecol Eng* 145:105740
- Zhang J, Wang Q, Mu W, Wei K, Guo Y, Sun Y (2022) Experimental investigation of the different polyacrylamide dosages on soil water movement under brackish water infiltration. *Polymers (basel)* 14:2495
- Zhao W, Hu J, Cui Z, Dou P, Fan Y (2019) Effects of superabsorbent polymers on the vertical infiltration of soil water with sand mulching. *Environ Earth Sci* 78:1–6
- Zhong K, Zheng X, Mao X, Lin Z, Jiang G (2012) Sugarcane bagasse derivative-based superabsorbent containing phosphate rock with water–fertilizer integration. *Carbohydr Polym* 90:820–826

Submit your manuscript to a SpringerOpen[®] journal and benefit from:

- ▶ Convenient online submission
- ▶ Rigorous peer review
- ▶ Open access: articles freely available online
- ▶ High visibility within the field
- ▶ Retaining the copyright to your article

Submit your next manuscript at ► [springeropen.com](https://www.springeropen.com)
